J Mater Sci (2015) 50:1770–1782
DOI 10.1007/s10853-014-8740-z

Mechanical properties of low-cost, earth-abundant chalcogenide thermoelectric materials, PbSe and PbS, with additions of 0–4 % CdS or ZnS

Robert D. Schmidt · Eldon D. Case · Li-Dong Zhao · Mercouri G. Kanatzidis

Received: 24 September 2014 / Accepted: 22 November 2014 / Published online: 2 December 2014

Abstract PbTe-based thermoelectric (TE) materials have been extensively investigated as TE generator materials, however, the tellurium content limits the application potential due to both availability and cost. Replacing the tellurium with selenium or sulfur produces an isomorphic TE material with very good reported figure of merit, *ZT*, values of 1.3–1.6, but the effect of the material changes designed to increase *ZT* (doping, nano- and micro-precipitate additions) on mechanical properties has not been reported. In order to effectively incorporate these new materials into TE devices, it is important to understand materials' response to thermally and mechanically imposed loads, which in turn requires knowledge of the mechanical properties. In this study, the hardness was determined by Vickers indentation and elastic modulus and Poisson's ratio were measured using resonant ultrasound spectroscopy on PbSe- and PbS-based TE specimens as a function the addition of 0–4 at.% of CdS or ZnS. With 2.0 or 2.5 at.% Na doping, the hardness of PbSe- or PbS-based TE materials increased by about 30 % and the elastic moduli decreased by 5–10 %. In addition, PbS may be effectively sintered at 723 K when doped with 2.5 at.% Na, but requires a higher sintering temperature when undoped. This study shows that the hardness and moduli of PbSe- or PbS-based TE materials are not strong functions of the addition of CdS or ZnS precipitates.

R. D. Schmidt (✉) · E. D. Case
Chemical Engineering and Materials Science Department, Michigan State University, 428 S. Shaw Lane, Room 3264, East Lansing, MI 48824, USA
e-mail: schmi402@msu.edu

E. D. Case
e-mail: casee@egr.msu.edu

L.-D. Zhao · M. G. Kanatzidis
Department of Chemistry, Northwestern University, Evanston, IL 60208, USA
e-mail: zhaolidong@buaa.edu.cn

M. G. Kanatzidis
e-mail: m-kanatzidis@northwestern.edu

L.-D. Zhao
School of Materials Science and Engineering, Beihang University, Beijing 100191, China

Introduction

The figure of merit, *ZT*, of bulk thermoelectric (TE) has been increased using a variety of techniques, particularly with lead telluride-based TEs with rock salt structure, with *ZT* values near or greater than 2 reported [1–3]. A limitation on the application of these high-*ZT* materials is the use of tellurium, due to the relative scarcity of the element [4], but sulfur or selenium may be substituted for tellurium to produce isomorphous (rock salt structure) compounds [1, 5–7] with demonstrated *ZT* values of 1.6 for lead selenide [1] and 1.3 for lead sulfide [6, 7]. However, the material changes to achieve these *ZT* values from PbS- and PbSe-based TE materials, namely by (i) doping and (ii) additions of precipitates can dramatically alter the mechanical properties of the material, as has been observed previously in lead telluride-based materials [8, 9]. The elastic properties of the TE materials are required to determine the material response to stresses, just as the transport properties are required to determine the *ZT* of the material. In waste heat harvesting applications, the stresses that the TE material must survive are not trivial, as TE materials are intended for an environment with thermal gradients, thermal shocks, attached to materials with thermal expansion mismatches, and subjected to external loads. The modeling

of the stress and strain by analytical or numerical methods such as finite element method, requires knowledge of the elastic moduli [10]. For example, in a simple slab plate in a steady state thermal gradient, the maximum stress σ_{max} is a function of Young's modulus, E,

$$\sigma_{max} = \frac{E\alpha}{(1-\nu)}\Delta T, \quad (1)$$

where α is the coefficient of thermal expansion, ν is Poisson's ratio, and ΔT is the temperature difference between the hot and cold sides of the plate [11].

The hardness of TE materials are related to the wear and machining characteristics [12]. In addition, the upper limit compressive strength σ_c is related to H and may be estimated as approximately $H/3$ [12, 13], especially useful in the design and fabrication of a module that may likely be intentionally in compression. Typically, TE materials have a relatively high mechanical strength in compression [14], a property that may be taken advantage of in design and fabrication of TE modules.

The mechanical properties of many undoped TE materials have been published, including PbS [15, 16] and PbSe [15, 17, 18], but the mechanical properties may be significantly changed when the TE material is optimized for improved ZT. The hardness and/or elastic moduli of a TE material have been shown to change by the addition of nanoparticles [19, 20], creation of nanoprecipitates in the bulk material [21], doping [22], or alloying [22, 23]. Therefore, to understand the mechanical response of a TE material that may be incorporated into a device, the mechanical properties need to be measured on a TE material with the addition of dopants, with nanoparticle or nanoprecipitates, rather than rely on mechanical property measurements of pure, undoped materials. This study examines the elastic moduli and hardness of PbS and PbSe, comparing the undoped mechanical properties to those doped with 2 or 2.5 % Na, respectively, and examining the influence of up to 4 % CdS or ZnS nanoprecipitate additions to the Na-doped material.

Experimental procedure

Materials and specimen preparation

Two tellurium-free TE materials with isomorphous crystal structure to PbTe-based TE materials (rock salt crystal structure) were included in this study, using methods similar to those employed to optimize the PbTe-based TE materials [1, 7]. Ingots were fabricated from elemental materials (99.99+ % purity) with nominal compositions of PbS or PbSe with x% CdS/ZnS, where the at fraction $x = 1$, 2, 3, and 4. For PbS, 2.5 at.% Na dopant was added [7] (Table 1), and for PbSe, 2.0 at.% Na dopant was added [1] (Table 2). In addition, ingots of PbS and PbSe without Na dopant, and an ingot of PbSe with 2.0 at.% Na dopant were made (Tables 1, 2). Carbon-coated fused silica tubes with the elemental material were evacuated to approximately 10^{-4} torr before being flame sealed [1, 7]. The tubes were heated to 723 K in 12 h, then to 1423 K in 7 h, thermally soaked for 6 h at 1423 K and then water quenched to room temperature [1, 7]. The ingots produced were crushed into powders, sieved through a 53-μm sieve, then densified by pulsed electric current sintering (PECS, Thermal Technology SPS-10-4 or SPS-DR 2050) at 723 K (PbS, doped and undoped), 873 K (undoped PbS) or 823 K (PbSe, doped and undoped) for 10 min in a 20 mm diameter graphite die under 60 MPa axial pressure in an argon atmosphere [1, 7]. Except for the undoped PbS sintered at 723 K, this produced highly dense disk-shaped billets 20 mm in diameter and 9 mm thick, with volume fraction porosity less than 0.05. Using a low speed diamond saw, the billets were cut into bars, ~2 mm × 3 mm in cross section and approximately 9–18 mm long [1, 7].

Elasticity measurements

In this study, the elastic moduli were determined by a standing acoustic wave technique, resonant ultrasound spectroscopy (RUS). The elastic moduli of each specimen are a function of the specimen geometry, dimensions, density, and resonant frequencies. Each of the specimens in this study was of rectangular bar geometry. The dimensions of each specimen were measured by micrometers (293-832, Mitutoyo, Japan), and the mass by electronic balance (Adventurer AR2140, OHAUS, Pine Brook, IL). The resonant frequencies were measured by RUS (RUSpec, Quasar International, Albuquerque, NM), in which the specimen was placed so that the corners of the specimen contacted two transducers along the specimen's body diagonal. One transducer was swept across a range of frequencies from 10 to 760 kHz in 29999 steps and the mechanical response to the frequency was recorded in the second transducer. Each sharp peak in second transducer's response to the driving signal (Fig. 1) represents a mechanical resonance frequency of the specimen. The set of recorded resonant frequencies were fit to a model by commercial software (RPModel version 2.68b, Quasar International) to determine the elastic moduli. Details of the RUS procedure may be found elsewhere [21, 24–27].

Hardness and toughness measurements

Hardness was measured by Vickers indentation at 1.98 N load on a microindenter (HMV-2000, Shimadzu, Okinawa, Japan), using the equation

Table 1 Composition, theoretical density, ρ_{theo}, measured density, ρ_{meas}, volume fraction porosity, P, average grain size, $\langle GS \rangle$, typical observed inclusion size range, Incl, for the PbS-based specimens included in this study

Composition	ρ_{theo} [a]	ρ_{meas}	P	$\langle GS \rangle$ (μm)	Incl (μm)
PbS	7.5970	7.535	0.008	5.9[b]	NA
$Pb_{0.975}Na_{0.025}S$	7.5970	7.325	0.036	1.8	NA
$Pb_{0.975}Na_{0.025}S$ + 1 at.% CdS	7.5716	7.278	0.039	3.2	0.2–1
$Pb_{0.975}Na_{0.025}S$ + 2 at.% CdS	7.5462	7.315	0.031	5.4	0.2–1.5
$Pb_{0.975}Na_{0.025}S$ + 3 at.% CdS	7.5207	7.148	0.050	4.5	0.2–2[c]
$Pb_{0.975}Na_{0.025}S$ + 4 at.% CdS	7.4952	7.148	0.046	3.6	0.2–3[c]
$Pb_{0.975}Na_{0.025}S$ + 1 at.% ZnS	7.5704	7.231	0.045	2.1	0.2–12
$Pb_{0.975}Na_{0.025}S$ + 2 at.% ZnS	7.5437	7.264	0.037	2.2	0.2–10[d]
$Pb_{0.975}Na_{0.025}S$ + 3 at.% ZnS	7.5168	7.241	0.037	2.3	0.2–15[d]
$Pb_{0.975}Na_{0.025}S$ + 4 at.% ZnS	7.4898	7.245	0.033	2.8	0.2–10

No inclusions because no addition of CdS or ZnS

NA not applicable

[a] The ρ_{theo} values are calculated in Table S1 from [6]

[b] The $\langle GS \rangle$ includes a distribution of several large grains, 5–30 μm, and smaller grains, 0.2–2 μm

[c] Inclusions were typically rod- or plate-like shape

[d] Larger inclusions were typically stacked plate-like shapes

Table 2 Composition, theoretical density, ρ_{theo}, measured density, ρ_{meas}, volume fraction porosity, P, average grain size, $\langle GS \rangle$, typical observed inclusion size range, Incl, for the PbSe-based specimens included in this study

Composition	ρ_{theo} [a]	ρ_{meas}	P	$\langle GS \rangle$ (μm)	Incl (μm)
PbSe	8.258	8.125	0.016	9.9	NA
$Pb_{0.98}Na_{0.02}Se$	8.258	7.955	0.037	4.0	NA
$Pb_{0.98}Na_{0.02}Se$ + 1 at.% CdS	8.2243	8.112	0.014	3.2	0.2–3
$Pb_{0.98}Na_{0.02}Se$ + 2 at.% CdS	8.1906	8.048	0.017	3.6	0.2–2
$Pb_{0.98}Na_{0.02}Se$ + 3 at.% CdS	8.157	7.950	0.025	4.0	0.2–3[b]
$Pb_{0.98}Na_{0.02}Se$ + 4 at.% CdS	8.1232	7.966	0.019	18.7	0.2–4[b]
$Pb_{0.98}Na_{0.02}Se$ + 1 at.% ZnS	8.2163	8.074	0.017	3.3	0.2–4
$Pb_{0.98}Na_{0.02}Se$ + 2 at.% ZnS	8.1746	8.005	0.021	3.2	0.2–10
$Pb_{0.98}Na_{0.02}Se$ + 3 at.% ZnS	8.1329	8.049	0.010	3.2	0.2–12
$Pb_{0.98}Na_{0.02}Se$ + 4 at.% ZnS	8.0912	7.880	0.026	7.0	0.2–15

No inclusions because no addition of CdS or ZnS

NA not applicable

[a] The ρ_{theo} values are calculated in Table S1 from [1]

[b] Inclusions were typically rod- or plate-like shape

$$H = \beta \frac{1.8544P}{(2a)^2}, \quad (2)$$

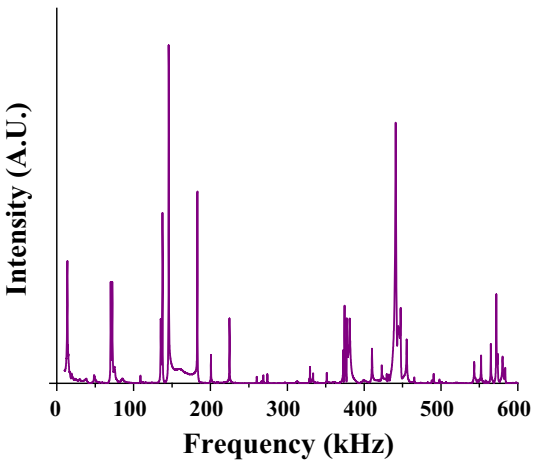

Fig. 1 RUS scan of PbSe specimen

where P is the indentation load and $2a$ is the length of the indentation diagonal [28]. The Vickers hardness values from indentation of a standard block (Yamamoto Scientific Tools Lab Co. Ltd, Chiba, Japan) were used to determine a calibration constant, β, of 0.95.

Microscopy and X-ray diffraction

The PbS and PbSe specimens were examined by scanning electron microscope (SEM) on both polished and fractured specimen surfaces at 15 kV accelerating voltage and 15 mm working distance (6610LV SEM, JEOL, Tokyo, Japan). Polished surfaces were examined by secondary electron

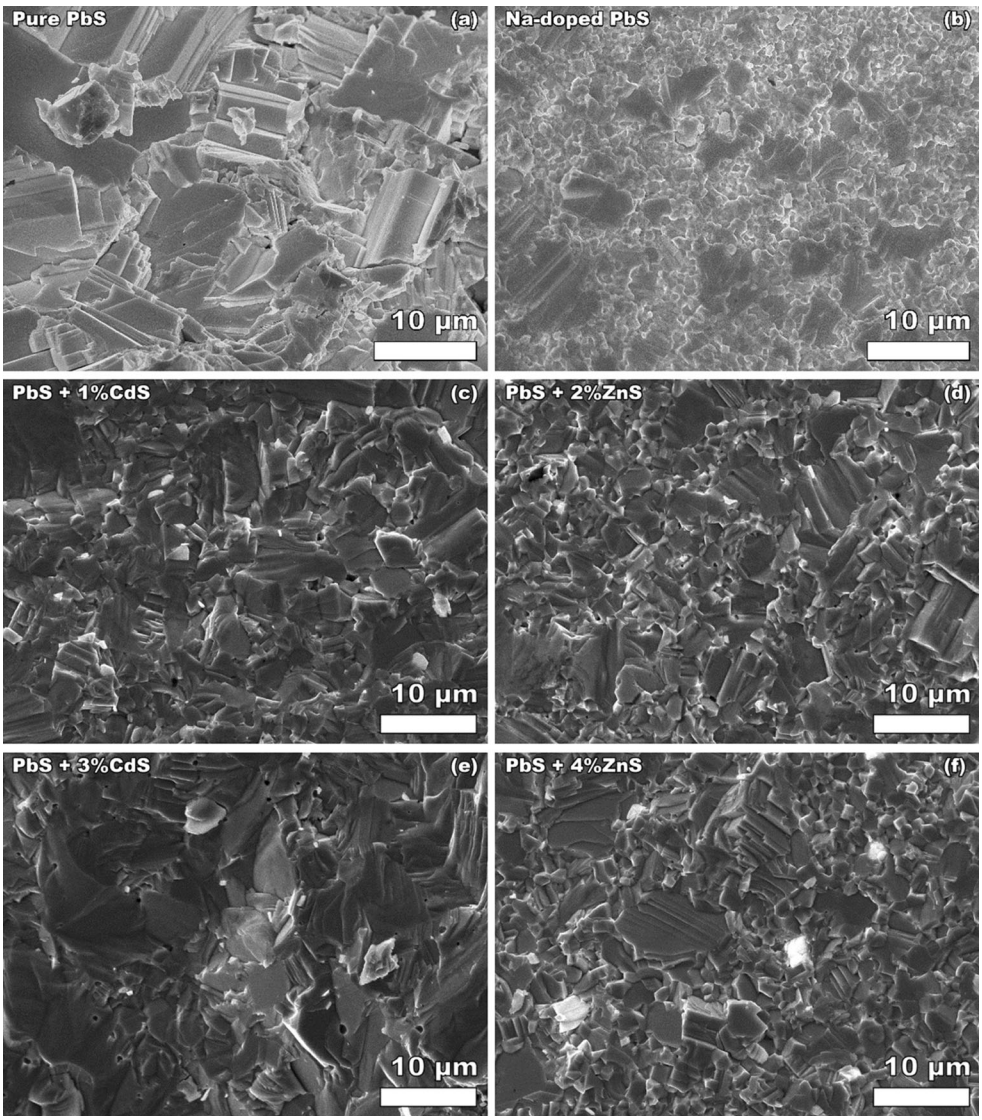

Fig. 2 Fracture surfaces of undoped PbS (**a**) changing to smaller average grain size for the Na-doped PbS specimen (**b**). With 1–4 % addition of CdS or ZnS (**c**–**f**) bright areas in images of precipitates are visible, particularly the ZnS precipitates (**d**, **f**)

images and backscatter images to examine indentation impressions and the morphology of secondary phases with different average atomic weight. Grain size analysis was performed by the linear intercept method on secondary electron images of fractured specimen surfaces, with a minimum of 200 intercepts per image and a stereographic projection factor of 1.5. Energy dispersive X-ray spectroscopy (Oxford EDS) was performed in the SEM at 15 kV accelerating voltage and 10 mm working distance for elemental analysis of five polished surface areas of PbS, where the area of each site was approximately 0.05 mm^2. Manufacturer library standards with a claimed accuracy of 25 % or less of the measurement were employed in EDS to determine the concentration of the elements.

X-ray diffraction (XRD) was performed at the Michigan State University Center for Crystallographic Research with Cu Kα radiation and a step size of 0.008° 2θ (Bruker Davinci Diffractometer) from 25° to 75° 2θ on a rotary stage. The XRD was performed on the bulk-densified PbS material.

Results and discussion

Microstructural analysis

Only isolated spherical porosity was observed in each of the specimens, consistent with specimens of densities greater than 95 % (Tables 1, 2). Except for 1 at.% ZnS in PbSe (with precipitates up to 4 μm), the addition of ZnS in PbS or PbSe resulted in ZnS precipitates with diameters up to 10–15 μm (Tables 1, 2), observed primarily at the grain boundaries (Figs. 2, 3, 4). The addition of 1–4 at.% CdS in

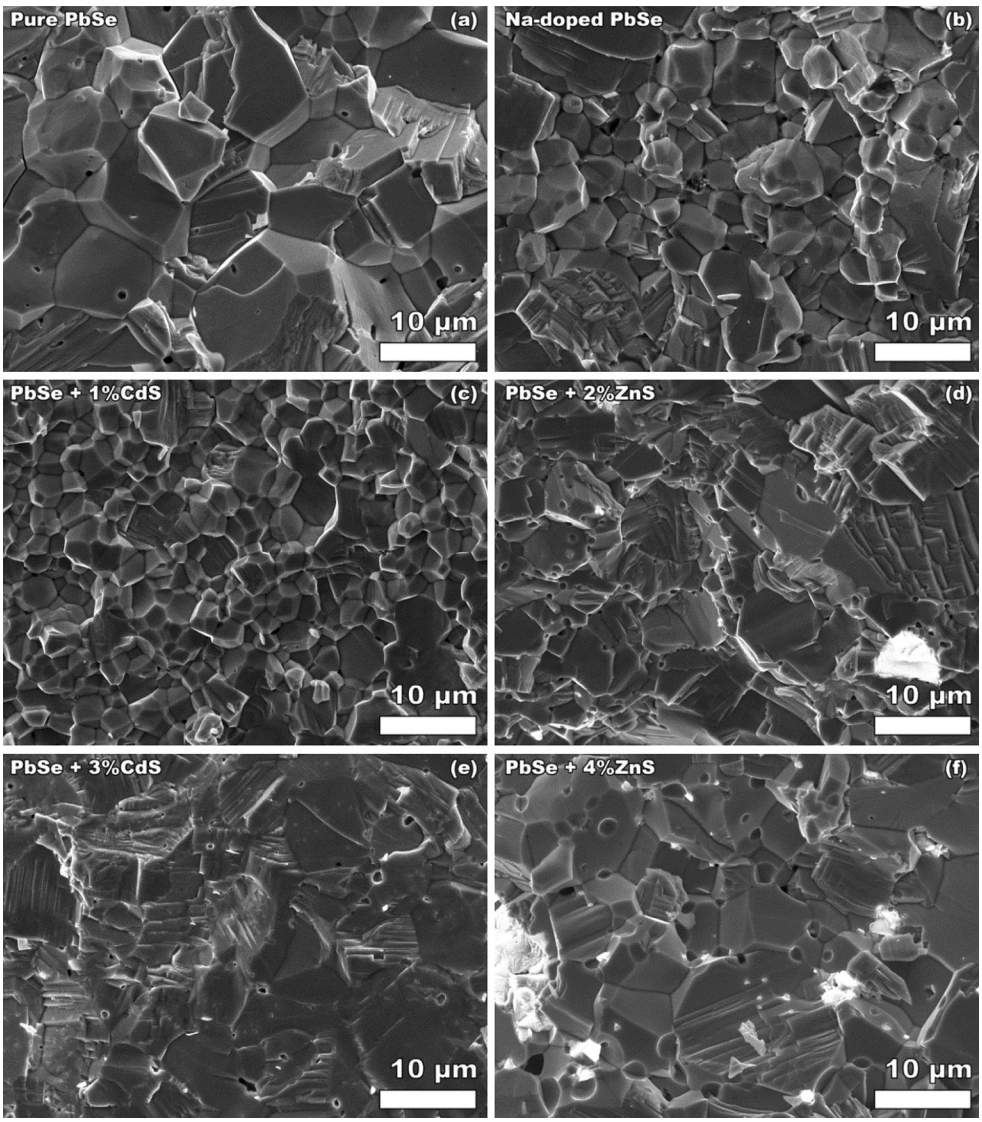

Fig. 3 Fracture surfaces of undoped PbSe (**a**), Na-doped PbSe (**b**), and with 1 % to 4 % CdS or ZnS precipitates (**c**–**f**). Note the *bright areas* in images (**d**) and (**f**) are the ZnS precipitates

PbS or PbSe resulted in precipitates with diameters of up to 1–4 μm (Tables 1, 2), observed primarily embedded in the matrix material (Figs. 2, 3, 4). In backscatter SEM imaging, both the CdS and ZnS precipitates were uniformly distributed through the specimen matrix, with up to 15 μm ZnS precipitates observed in both the PbSe and PbS (Fig. 4; Tables 1, 2). No precipitates were observed in the samples of either PbS or PbSe without CdS or ZnS additions. All the precipitates observed in this study were faceted (Figs. 4, 5). In particular, the precipitate morphology was rod- or plate-like for the CdS additions in both PbS and PbSe (Fig. 5). In addition, the ZnS precipitate morphology included stacked plates, particularly in the PbS matrix (Figs. 4, 6).

EDS analysis of the polished surface of PbS indicated a possible deficiency of S (Table 3), although the results from EDS are not sufficiently accurate to determine stoichiometry. However, the question of stoichiometry can be examined further using X-ray diffraction. The lattice parameter from XRD of the PbS specimen was 0.59409 ± 0.00004 nm for the bulk, as-sintered specimen (Fig. 7). The measured lattice parameter for sintered PbS is larger than the lattice parameter of 0.5932 nm for the same PbS material prior to sintering [6], and larger than the published room temperature lattice parameter of 5.9315 Å [29]. The larger lattice parameter of the sintered specimen is consistent with a change in the concentration of S. The implications of S vacancies are discussed in "Elasticity analysis" section.

The undoped PbS specimen required a higher sintering temperature (873 K) than the Na-doped PbS specimens (723 K). An undoped PbS specimen produced at a sintering temperature of 723 K was too porous for comparison to the

nearly dense Na-doped specimens, with a density of 6.27 g/cm^3, and a P of 0.18, far exceeding the maximum of $P < 0.05$ for all other specimens in this study. Therefore, the porous undoped PbS specimen was excluded from the elasticity and hardness testing.

Elasticity results

For the PbS-based specimens, the elastic moduli, E and G, were not sensitive to the addition of CdS or ZnS, with a mean and standard deviation of E of 63.38 ± 2.25 GPa (Fig. 8a) and G was 24.69 ± 0.93 GPa (Fig. 8c). The undoped PbS specimen had a much lower porosity, $P = 0.008$, than all the other Na-doped PbS-based specimens, $P = 0.031$–0.050 (Table 1), likely due to the higher sintering temperature of the PbS specimen (see "Materials and specimen preparation" section for sintering procedures). This difference in P likely explains the higher E and G of the undoped PbS specimen relative to the other PbS-based specimens (Fig. 8a), and not a sensitivity to Na doping, as discussed in "Elasticity analysis" section.

In contrast, the moduli of the PbSe-based specimens are sensitive to Na doping, but not CdS or ZnS additions. Both the E and G of the PbSe specimens decreased with the addition of Na dopant, from 64.29 ± 0.16 and 25.29 ± 0.02 GPa for pure PbSe, to 60.33 ± 0.26 and 23.66 ± 0.04 GPa for Na-doped PbSe (Fig. 8b, d). No change in modulus was observed

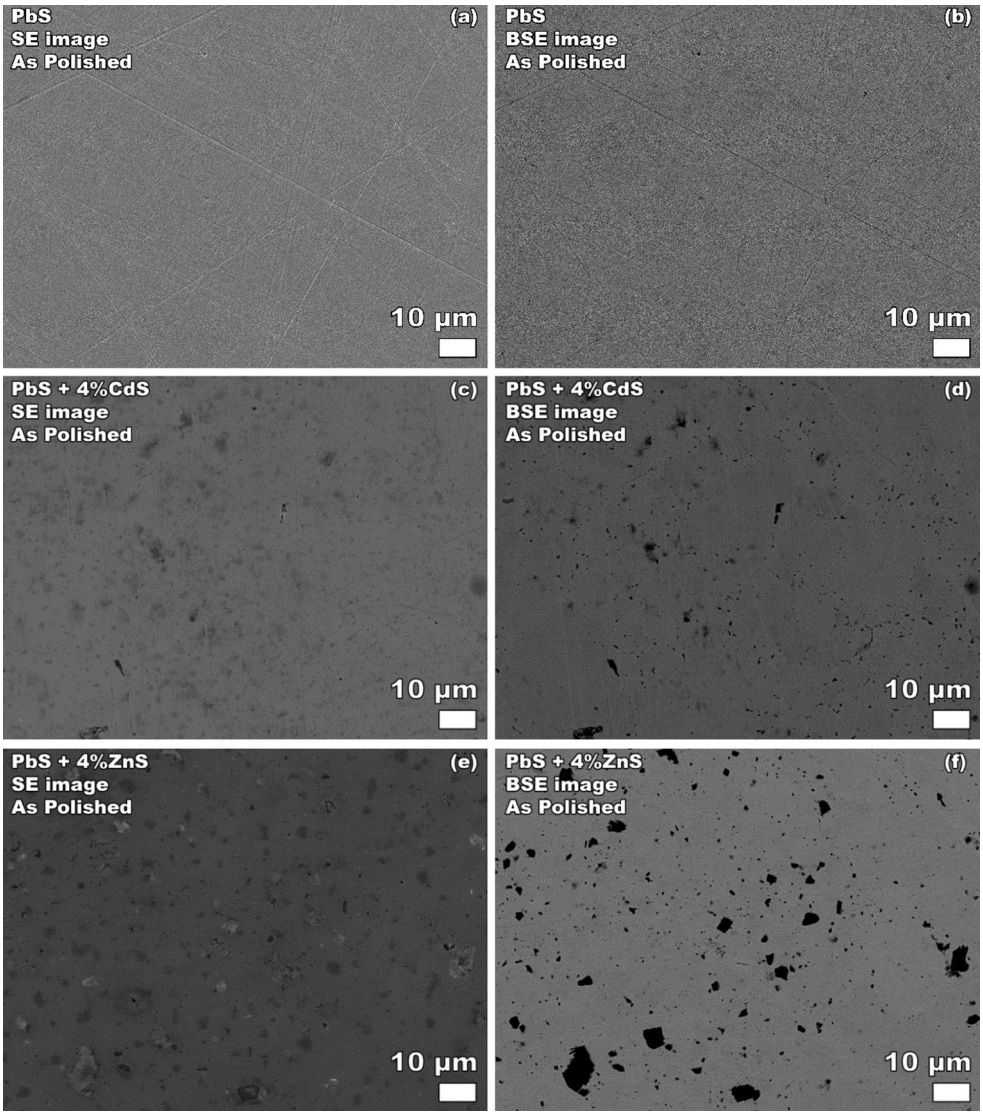

Fig. 4 Secondary electron SEM images of the polished specimens show isolated, micron-scale spherical porosity, and minor scratches from polishing. In the PbS specimens with 4 % CdS (**c**, **d**) or ZnS (**e**, **f**) and the PbSe specimens with 4 % CdS (**g**, **h**) or ZnS (**i**, **j**), precipitates of sub-micron up to approximately 15 µm were observed, particularly in backscatter electron (BSE) mode (**b**, **d**, **f**, **h**, **j**). The images of polished PbS in both secondary electron (SE) and BSE mode (**a**, **b**) only exhibit spherical pores ~1 µm, with no evidence of precipitates, consistent with the material having no additions of CdS or ZnS

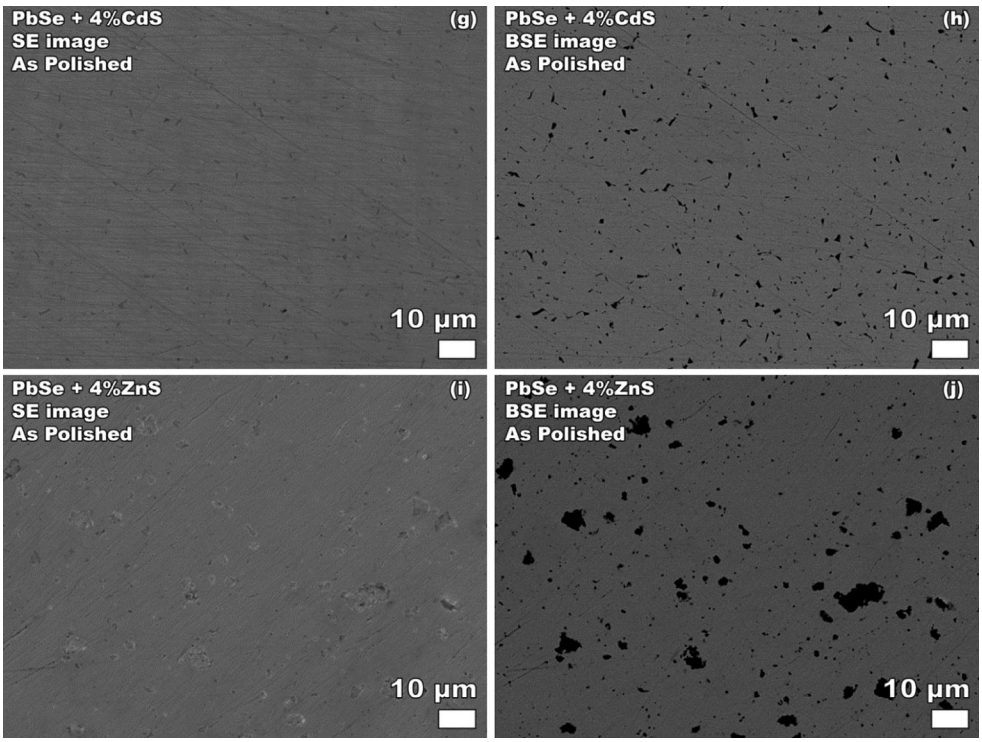

Fig. 4 continued

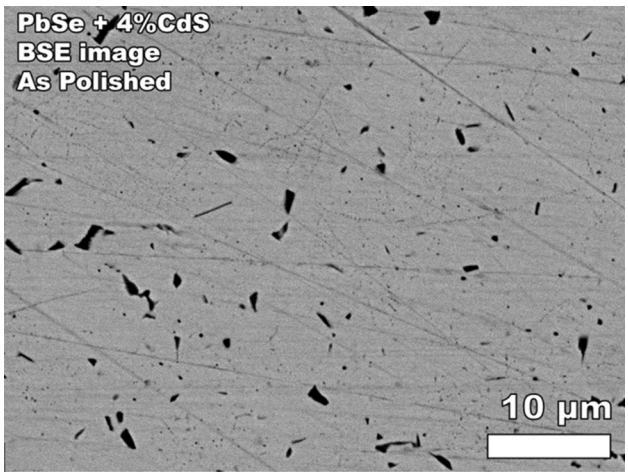

Fig. 5 Observed in backscattered electron mode, precipitates of CdS were up to ~4 μm, with some micron-scale precipitates with geometry of rods or plates and sharp facets consistent with crystallographic alignment

in the Na-doped PbSe specimens as a function of increasing additions of 1–4 at.% CdS or ZnS except for a slight decrease in G and a corresponding increase in v. The mean of E for the PbSe specimens with either CdS or ZnS was 61.03 ± 0.79 and the mean of G was 23.35 ± 0.35 GPa) (Fig. 8b, d, f). (Note: each of the specimens with additions of CdS or ZnS was Na-doped.)

Hardness results

The hardness of PbS and PbSe increased with 2.5 or 2.0 at.% Na-dopant additions, respectively, but were largely unaffected by the addition of 0–4 at.% CdS or ZnS (Fig. 9). The hardness of the pure PbS was 0.72 ± 0.10, and the average of the Na-doped PbS with additions of 0–4 at.% CdS or ZnS was 1.12 ± 0.05 (Fig. 9a). Similarly, the hardness of the pure PbSe was 0.44 ± 0.02 GPa, but increased to 0.62 ± 0.02 GPa when doped with 2.0 at.% Na, and averaging 0.74 ± 0.08 GPa for specimens with 0–4 at.% CdS or ZnS (Fig. 9b).

Discussion

Microstructural analysis

The observation of ZnS precipitates of up to 10–15 μm in diameter (Tables 1, 2), as compared to CdS precipitates of up to 1.5–4 μm in both the PbS matrix (Table 1; Fig. 4) and the PbSe matrix (Table 2; Fig. 4), may be related to the much lower solubility limit of ZnS in the matrix [1]. More specifically for PbSe, "no solid solubility of Zn in PbSe was observed" [1]. Zhao et al. expected a continuous change in band gap up to the solubility limit for additions of CdS or ZnS in PbSe [1]. The band gap increased with up

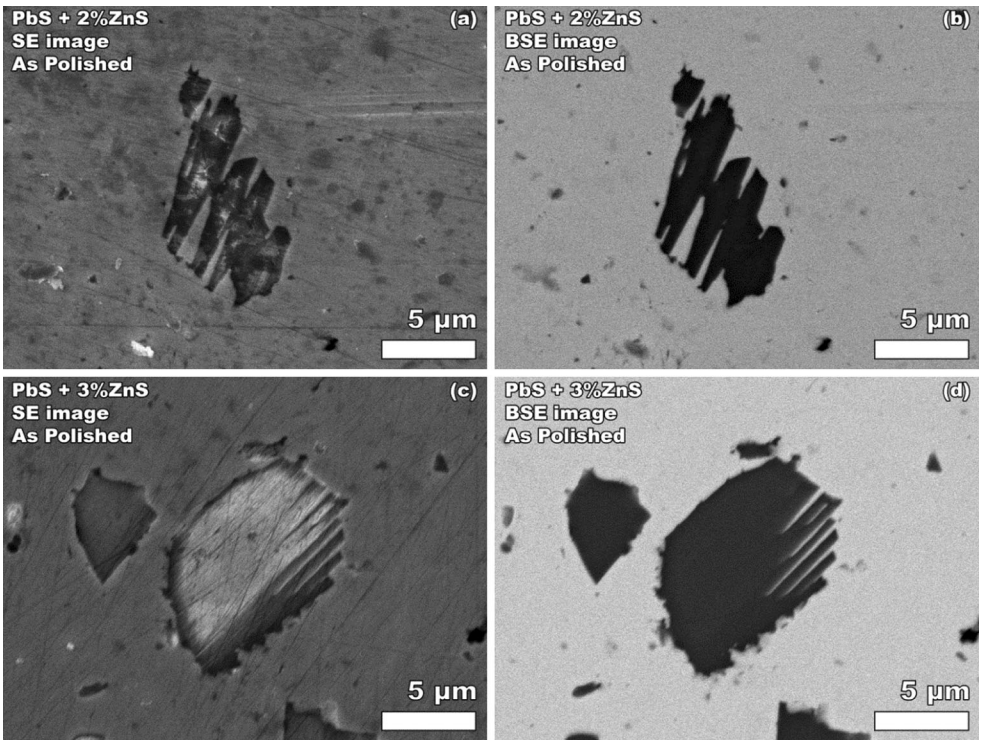

Fig. 6 SEM image of ZnS inclusions in PbS showing "stacked plate" morphology

Table 3 EDS results from four area scans of a polished PbS specimen, indicating a higher concentration of Pb than S

Location ID	At.%	
	S	Pb
1	49.6	50.4
2	49.6	50.4
3	49.1	50.9
4	49.5	50.5
5	49.2	50.8

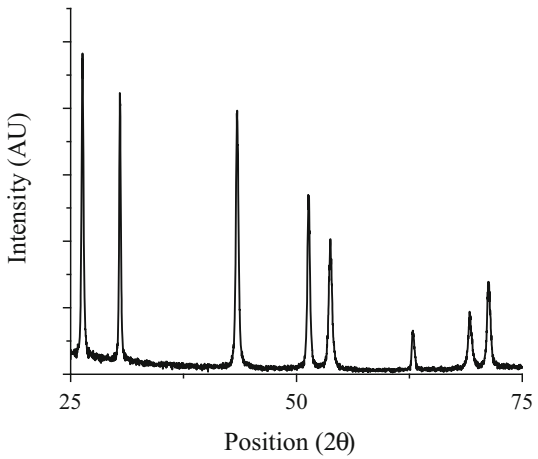

Fig. 7 XRD pattern of the sintered PbS specimen

to 2 % addition of CdS in PbSe, but with ZnS in PbSe, "no band gap changes are observed, suggesting a much lower solubility limit" of ZnS in PbSe [1].

Transmission electron microscopy observations of nanoprecipitates of CdS and ZnS in PbS and PbSe matrices have shown endotaxial crystallographic alignment with the matrix [1, 6]. The morphology of the observed micron-scale precipitates with rod or plate geometry and sharp facets (Fig. 4), particularly in the samples with CdS addition (Fig. 5), are consistent with the observations of nanoprecipitate morphology.

For PbS-based specimens sintered at 723 K, the P for the undoped material was 0.18, while the P of each of the Na-doped specimens was less than 0.05. A nearly dense ($P = 0.01$) undoped PbS specimen was sintered for this study, but only by increasing the sintering temperature to 873 K. The enhanced densification of the Na-doped PbS specimens may indicate the Na dopant acts as a sintering aid. A previous study on a different TE material, $Ba_{0.3}Co_4Sb_{12}$, showed the addition of metal particles, specifically 0.5 wt% Ag nanoparticles, may act as sintering aid [30]. In $Ba_{0.3}Co_4Sb_{12}$, the Ag had a eutectic or peritectic reaction with Sb in the $Ba_{0.3}Co_4Sb_{12}$ [30] and a similar eutectic reaction may explain the enhanced densification in the Na-doped PbS specimens.

The Na–S system has eutectics at 513 K and 61.5 at.% Na, 522 K and 70 at.% Na, and at 525 K and 72.5 at.% Na

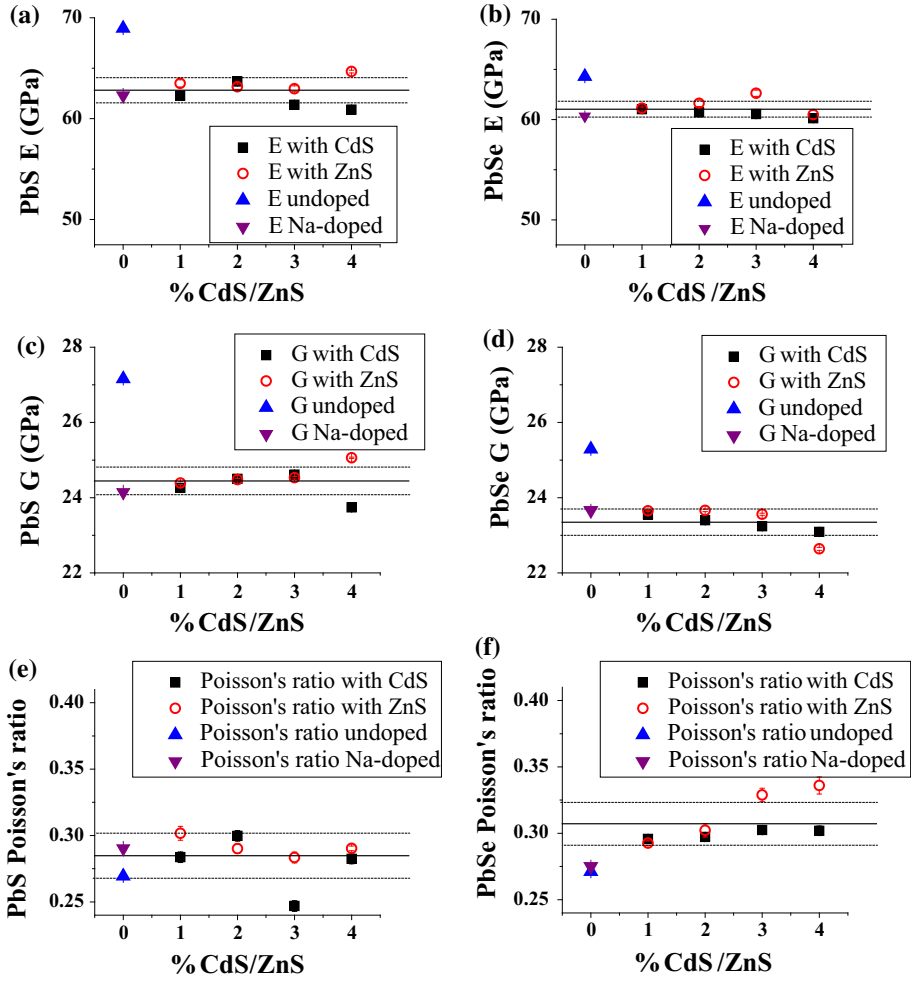

Fig. 8 The E and G of the undoped PbS and PbSe were higher than the Na-doped PbS and PbSe. The E and G of undoped PbS are likely higher due to reduced porosity (pure PbS $P = 0.008$, all other PbS $P = 0.031$–0.050), while the E and G of undoped PbSe are likely higher due to doping effects. Only small changes in E and G were noted in Na-doped PbS and PbSe with addition of up to 4 % CdS or ZnS. Only small variability in the ν noted in PbS with addition of CdS or ZnS. The ν of PbSe increased with the addition of CdS or ZnS. *Solid line* is average and *dotted line* is standard deviation of the specimens with 1–4 % CdS or ZnS addition

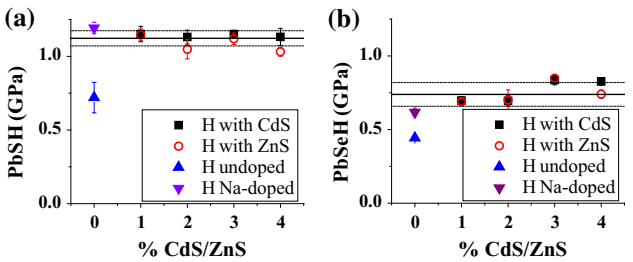

Fig. 9 The hardness of both PbS and PbSe increased with the addition of Na dopant. No measurable change in hardness was noted in PbS with addition of up to 4 % CdS or ZnS. Hardness of PbSe increased from 0.6 to 0.8 GPa with the addition of either CdS or ZnS

[31]. All three of these eutectic points are well below the sintering temperature used for the Na-doped PbS samples, 723 K. In the closely related PbTe material system, the Na in Na-doped PbTe partially segregates in a layer less than 10 nm thick at the grain boundaries [2]. A similar Na-rich layer may also form during sintering in the PbS-based material in this study, and this Na-rich layer may act as a liquid-phase sintering aid for the PbS-based system that accounts for the enhanced sintering. The sintering behavior of Na-doped PbS has not been explored and may be a topic for future work.

Elasticity analysis

For the PbS-based specimens, the undoped PbS specimen exhibited higher E and G relative to the other PbS-based specimens (Fig. 8a). The difference in elastic moduli among PbS-based specimens is likely a function of porosity, as the porosity of the undoped PbS specimen is $P = 0.008$, much lower than all the other Na-doped PbS-based specimens, $P = 0.031$–0.050 (Table 1), and not because of a sensitivity to the Na doping.

In general, the elastic modulus of TE materials and other brittle materials is a linear function of porosity [12, 27, 32, 33],

$$E = E_0(1 - b_E P), \tag{3}$$

where E_0 is the Young's modulus at $P = 0$, and b_E is a measure of the decrease in E with increasing P. For two

previously studied TE materials, $YbAl_3$ and lead–antimony–silver–tellurium (LAST), b_E is 2.34 [27] and 3.6 [32]. Based on these values of b_E, the difference between the undoped PbS and the Na-doped specimens with 0–4 at.% addition of CdS or ZnS is expected to be between 4 and 11 GPa, and consistent with the measured difference of approximately 6 GPa (Fig. 8a).

The elastic moduli for the doped TE materials with nanoprecipitates in this study have not been reported, however, the moduli of the undoped PbS [15, 16] and PbSe [15, 17, 18] are known for single crystal specimens. The aggregate average of the Hashin and Shtrikman bounds, ⟨H–S⟩, [34] allow a direct comparison of the single crystal specimen moduli to the moduli of a dense polycrystalline specimen (Table 4). Comparing this study to the ⟨H–S⟩ averages, the polycrystalline PbS specimen in this study (which has a volume fraction porosity, P of 0.008) were lower than the single crystal values by 12–18 %, with the measured E of 68.95 ± 0.10 GPa in this study, and the single crystal ⟨H–S⟩ E of 78.05 GPa [15] and 83.61 GPa [16] (Table 4). The elastic moduli of PbSe in this study ($P = 0.016$), with E of 64.29 ± 0.16 GPa, generally agrees with previous studies, with ⟨H–S⟩ E between 61.68 and 70.69 GPa [15, 17, 18] (Table 4).

The reader may ask, "why are the moduli of PbS lower than those reported in literature?" The two most likely causes would be (i) porosity and (ii) doping or composition differences.

Porosity is not sufficient by itself to explain the difference between the literature values of ⟨H–S⟩ E and the measured E in this study. The contribution from porosity may be estimated using Eq. 3 and applying the measured b_E from two previously studied TE materials, $YbAl_3$ ($b_E = 2.34$) [27] and LAST ($b_E = 3.6$) [32]. Based on these values of b_E and the observed porosity in the PbS specimen ($P = 0.046$), the E_0 of PbS in this study would likely be in the range of 70.3–71.0 GPa, which is still 12–15 % less than the average of literature values (Table 4).

After accounting for porosity, the remaining differences between the moduli of the polycrystalline PbS specimen in this study and the literature may be related to composition or doping and vacancies. The EDS surface composition of a polished surface of the specimen was $PbS_{0.98}$, averaged over five separate sites (Table 3). However, the small concentration of S vacancies indicated (Table 3) is within the error of the EDS technique, and insufficient to claim S vacancies by EDS analysis alone. Nevertheless a change in vacancy concentration of this magnitude should be discernable in terms of changes in lattice parameter of PbS. Prior to sintering, the powder was single phase in XRD, with a lattice parameter of 0.5932 nm [6], consistent with published values for the lattice parameter of PbS at room temperature [29]. After sintering, the specimen was single phase in XRD, but with a lattice parameter of 0.5941 nm (Fig. 7). The increase in lattice parameter is consistent with a change in vacancy concentration. In this study, the PbS was densified by PECS in an argon atmosphere using a starting powder milled from an ingot. During the initial stage of sintering before densification occurs, the surfaces of the PbS powder particles are exposed to the sintering atmosphere at elevated temperature, 873 K, providing a pathway for S loss. Thus, the observed reduction in the elastic moduli by roughly 12–15 % in this study may be caused by sulfur vacancies introduced during sintering.

A change in elastic moduli by roughly 12–15 % due to vacancies is not unique to PbS. Another TE material, $SnTe_{1+x}$, exhibits a decrease of E by 12 % with increasing TE content from $x = 0$–0.016 and a subsequent rise in the number of cation vacancies [35]. In addition, the elastic modulus of a set of nitrides decreases with increasing N vacancies. The E of TiN_x coatings decreases by 23 % [36] or 41 % [37] for a change in x from 1 to 0.67, decreases ~20 % [38] or 50 % [37] for x from 1 to 0.5, and by 5 % for a small change of x from 0.98 to 0.94 [37]. Similarly, the E of ZrN_x decreased 12 % for a change in x from 1 to 0.85 [37]. For CeO_{2-x}-based compounds, increasing O

Table 4 The Young's modulus, E, the shear modulus, G, and the Poisson's ratio measured in this study for the polycrystalline undoped PbSe and undoped PbS specimens compared with the aggregate average values of E and G computed from the Hashin and Shtrikman bounds, ⟨H–S⟩ [34] for single crystal elasticity from the literature [15–18]

Material	Bulk material form	E (GPa)	G (GPa)	Poisson's ratio	Density (g/cm^3)	Reference
PbS	Polycrystalline	68.95	27.16	0.269	7.53	This study
PbS	Single crystal	78.05	29.98	0.302	7.5 ($P = 0.01$)	[15]
PbS	Single crystal	83.61	32.53	0.277	NA	[16]
PbSe	Polycrystalline	64.29	25.29	0.271	8.13	This study
PbSe	Single crystal	66.83	23.76	0.298	8.26	[17]
PbSe	Single crystal	70.69	24.11	0.466	8.16 ($P = 0.01$)	[15]
PbSe	Single crystal	61.68	23.76	0.294	NA	[18]

NA not available from literature

Table 5 In general, hardness, H, is grain size dependent, and the single crystal hardness results from Bloem and Kröger [40] are expected to have a lower hardness than the other, polycrystalline specimens in this table

Material	Bulk material form	H (GPa)	Indentation Load (N)	Reference
PbS	Polycrystalline	1.09 ± 0.14	1.96	This study
PbS	Single crystal	0.4–0.7 (dependent on vacancy concentration)	0.98	[40]
PbS	Polycrystalline	0.72–0.92	1.41	[23]
PbS	Polycrystalline	0.73	3.92	[23]
PbSe	Polycrystalline	0.44 ± 0.02	1.96	This study
Na-doped PbSe	Polycrystalline	0.62 ± 0.02	1.96	This study
PbSe	Polycrystalline	0.56–0.57	1.41	[23]

The grain size for the PbS and PbSe was not listed by Darrow [28]. Average grain sizes for all specimens in this study are between 1.8 and 18.7 μm, listed in Tables 1 and 2

vacancies (x from approximately 0 to approximately 0.11, at O_2 partial pressure of 0.22 atm and 4.50×10^{-22} atm) reduced the E of ceria by 11 % and gadolinium doped ceria by 6 % [39].

Hardness analysis

Hardness values for single crystal PbS [23, 40] and polycrystalline specimens of PbS and PbSe [23] are available in the literature (Table 5), but no hardness data is available in the literature for PbS and PbSe specimens optimized as TE materials by the inclusion of Na dopant and CdS or ZnS nano/micro precipitates.

The hardness of PbS specimens included in this study was not observed to be a function of addition of precipitates or the dopant (Table 5; Fig. 9a). The hardness of PbS is higher than reported in the literature [23, 40], but hardness is known to be a function of grain size, and would be expected to be higher for the powder processed specimens in this study than for single crystal specimens of the same composition [41].

Although the hardness was not observed to be a function of Na doping in this study, the hardness of PbS is a function of the vacancy concentration [40]. On single crystal specimens of PbS, Bloem and Kröger reported a minimum hardness of 0.4 GPa is reported when there is a minimum of vacancies [40]. In this study, the PbS was S-deficient ("Elasticity analysis" section; Table 3), implying S vacancies were present, regardless of the Na doping and regardless of whether or not CdS or ZnS was added to the matrix. The difference between the constant H in this study and the minimum reported by Bloem and Kröger [40] is likely because there are likely a large number of S vacancies (Table 3) in each of the PbS specimens in this study. For future work with different processing conditions or Na doping concentrations, the vacancy concentration may approach a value where a minimum in H is possible, and the value of H should be reexamined.

For PbSe, there may be a similar relationship between vacancies and hardness as was observed by Bloem and Kröger in PbS [40]. Without CdS or ZnS additions, the hardness increased from 0.44 ± 0.02 to 0.62 ± 0.02 GPa with the addition of 2.0 at.% Na dopant (Table 5; Fig. 9b). After the addition of Na, the hardness was only a weak function, if any, of CdS or ZnS addition, averaging 0.75 ± 0.07 GPa for all the specimens with CdS or ZnS addition (Fig. 9b).

Conclusions

The effects on mechanical properties of PbS and PbSe from two aspects of ZT optimization were examined in this study, (i) addition of a precipitate phase, namely CdS or ZnS, and (ii) changes based on Na doping or S deficiency. In particular, the elastic moduli and H of PbS are not functions of either (i) the CdS or ZnS addition or (ii) the Na dopant. The elastic moduli of the sintered pure PbS ($E = 68.95$ GPa) are lower than previous reports ($E = 78.05$ GPa [15], 83.61 GPa [16]), which is likely related to S vacancies. However, a decrease in the sintering temperature suggests that Na may act as a sintering aid.

For PbSe, elastic moduli and H are not functions of the CdS or ZnS addition. However, both the elastic moduli and hardness of PbSe are functions of the 2.0 at.% Na dopant. Without the Na dopant, the E was 64.29 ± 0.16 GPa and H was 0.44 ± 0.02 GPa. With the Na dopant, the averaged E was 61.03 ± 0.79 and the average H was 0.75 ± 0.07 GPa.

Thus, optimizing the ZT of either PbS or PbSe by addition of up to 4 at.% CdS or ZnS may be performed without concern for changing elastic moduli or H, but the addition of Na alters the elastic moduli and H of PbSe and the sintering behavior of PbS.

From the experimental results of this study, a designer of a TE module based on PbS or PbSe may vary the

addition of precipitates of CdS or ZnS with no appreciable difference in the stress–strain behavior since the elastic moduli are unaffected by the precipitate addition. Likewise, since the hardness is not sensitive to the CdS or ZnS addition, no difference would be expected in the wear and machining characteristics. Furthermore in PbSe, a designer may have the freedom to determine the best Na doping level in terms of TE behavior with no difference in the stress–strain behavior, or the wear and machining characteristics. Like PbSe, no appreciable difference in the wear and machining characteristics is expected in PbS when doped with Na. However, in PbS, a decrease in the elastic modulus of about 12–24 % relative to single crystal measurements may occur due to the combined influence of S vacancies and Na doping, although the Na doping may lower the sintering temperature.

Acknowledgements The authors acknowledge the financial support of the Department of Energy, Revolutionary Materials for Solid State Energy Conversion Center, an Energy Frontiers Research Center funded by the U.S. Department of Energy, Office of Science, Office of Basic Energy Sciences under award number DE-SC0001054.

References

1. Zhao L-D, Hao S, Lo S-H et al (2013) High thermoelectric performance via hierarchical compositionally alloyed nanostructures. J Am Chem Soc 135:7364–7370. doi:10.1021/ja403134b
2. Biswas K, He J, Blum ID et al (2012) High-performance bulk thermoelectrics with all-scale hierarchical architectures. Nature 489:414–418. doi:10.1038/nature11439
3. Heremans JP, Jovovic V, Toberer ES et al (2008) Enhancement of thermoelectric efficiency in PbTe by distortion of the electronic density of states. Science 321:554–557. doi:10.1126/science.1159725
4. Haxel GB, Hedrick JB, Orris GJ (2002) Rare earth elements—critical resources for high technology. USGS Fact Sheet fs087-02. http://pubs.usgs.gov/fs/2002/fs087-02. Accessed 25 Apr 2014
5. Johnsen S, He J, Androulakis J et al (2011) Nanostructures boost the thermoelectric performance of PbS. J Am Chem Soc 133:3460–3470. doi:10.1021/ja109138p
6. Zhao L-D, He J, Hao S et al (2012) Raising the thermoelectric performance of p-type PbS with endotaxial nanostructuring and valence-band offset engineering using CdS and ZnS. J Am Chem Soc 134:16327–16336. doi:10.1021/ja306527n
7. Zhao L-D, He J, Wu C-I et al (2012) Thermoelectrics with earth abundant elements: high performance p-type PbS nanostructured with SrS and CaS. J Am Chem Soc 134:7902–7912. doi:10.1021/ja301772w
8. Ren F, Case ED, Timm EJ, Schock HJ (2007) Young's modulus as a function of composition for an n-type lead–antimony–silver–telluride (LAST) thermoelectric material. Philos Mag 87:4907–4934. doi:10.1080/14786430701589376
9. Ren F, Hall BD, Ni JE et al (2011) Mechanical characterization of PbTe-based thermoelectric materials. MRS Proc 1044:1044–1048. doi:10.1557/PROC-1044-U04-04
10. Kaliakin VN (2002) Introduction to approximate solution techniques, numerical modeling, and finite element methods. Marcel Dekker, New York
11. Kingery WD, Bowen HK, Uhlman DR (1976) Introduction to ceramics, 2nd edn. Wiley, New York
12. Rice RW (1998) Porosity of ceramics. Marcel Dekker, New York
13. Ren F, Case ED, Timm EJ, Schock HJ (2008) Hardness as a function of composition for n-type LAST thermoelectric material. J Alloys Compd 455:340–345. doi:10.1016/j.jallcom.2007.01.086
14. Hamid Elsheikh M, Shnawah DA, Sabri MFM et al (2014) A review on thermoelectric renewable energy: principle parameters that affect their performance. Renew Sustain Energy Rev 30:337–355. doi:10.1016/j.rser.2013.10.027
15. Dalven R (1969) A review of the semiconductor properties of PbTe, PbSe, PbS and PbO. Infrared Phys 9:141–184. doi:10.1016/0020-0891(69)90022-0
16. Bhagavantam S, Rao TS (1951) Elastic constants of Galena. Nature 168:42. doi:10.1038/168042b0
17. Lippmann G, Kästner P, Wanninger W (1971) Elastic constants of PbSe. Phys Status Solidi 6:K159–K161. doi:10.1002/pssa.2210060264
18. Hellwege K (1979) Landold–Bornstein numerical data and functional relationships in science and technology, new series, vol 11. Springer, Berlin
19. Zhao L-D, Zhang B-P, Li J-F et al (2008) Thermoelectric and mechanical properties of nano-SiC-dispersed Bi_2Te_3 fabricated by mechanical alloying and spark plasma sintering. J Alloys Compd 455:259–264. doi:10.1016/j.jallcom.2007.01.015
20. Kvetková L, Duszová A, Kašiarová M et al (2013) Influence of processing on fracture toughness of Si_3N_4+ graphene platelet composites. J Eur Ceram Soc 33:2299–2304. doi:10.1016/j.jeurceramsoc.2013.01.025
21. Ni JE, Case ED, Khabir KN et al (2010) Room temperature Young's modulus, shear modulus, Poisson's ratio and hardness of PbTe–PbS thermoelectric materials. Mater Sci Eng B 170:58–66. doi:10.1016/j.mseb.2010.02.026
22. Gelbstein Y, Gotesman G, Lishzinker Y et al (2008) Mechanical properties of PbTe-based thermoelectric semiconductors. Scripta Mater 58:251–254. doi:10.1016/j.scriptamat.2007.10.012
23. Darrow MS, White WB, Roy R (1969) Micro-indentation hardness variation as a function of composition for polycrystalline solutions in the systems PbS/PbTe, PbSe/PbTe, and PbS/PbSe. J Mater Sci 4:313–319. doi:10.1007/BF00550400
24. Ren F, Case ED, Ni JE et al (2009) Temperature-dependent elastic moduli of lead telluride-based thermoelectric materials. Philos Mag 89:143–167. doi:10.1080/14786430802607119
25. Schmidt RD, Ni JE, Case ED et al (2010) Room temperature Young's modulus, shear modulus, and Poisson's ratio of $Ce_{0.9}Fe_{3.5}Co_{0.5}Sb_{12}$ and $Co_{0.95}Pd_{0.05}Te_{0.05}Sb_3$ skutterudite materials. J Alloys Compd 504:303–309. doi:10.1016/j.jallcom.2010.06.003
26. Migliori A, Sarrao JL (1997) Resonant ultrasound spectroscopy: applications to physics, materials measurements, and nondestructive evaluation. Wiley-VCH, New York
27. Schmidt RD, Case ED, Lehr GJ, Morelli DT (2013) Room temperature mechanical properties of polycrystalline $YbAl_3$, a promising low temperature thermoelectric material. Intermetallics 35:15–24. doi:10.1016/j.intermet.2012.11.019
28. Wachtman JB, Cannon WR, Matthewson MJ (2009) Mechanical properties of ceramics, 2nd edn. Wiley-VCH, Hoboken
29. Noda Y, Masumoto K, Ohba S et al (1987) Temperature dependence of atomic thermal parameters of lead chaleogenides, PbS, PbSe and PbTe. Acta Crystallogr C43:1443–1445
30. Schmidt RD, Case ED, Lobo Z et al (2014) Influence of silver nanoparticle addition, porosity, and processing technique on the mechanical properties of $Ba_{0.3}Co_4Sb_{12}$ skutterudites. J Mater Sci 49:7192–7212. doi:10.1007/s10853-014-8427-5
31. Sangster J, Pelton AD (1997) The Na–S (sodium–sulfur) system. J Phase Equilib 18:89–96. doi:10.1007/BF02646762

32. Ni JE, Ren F, Case ED, Timm EJ (2009) Porosity dependence of elastic moduli in LAST (lead–antimony–silver–tellurium) thermoelectric materials. Mater Chem Phys 118:459–466. doi:10.1016/j.matchemphys.2009.08.018
33. Ni JE, Case ED, Stewart R et al (2011) Bloating in $(Pb_{0.95}Sn_{0.05}Te)_{0.92}(PbS)_{0.08}$–0.055%$PbI_2$ thermoelectric specimens as a result of processing conditions. J Electron Mater 41:1153–1158. doi:10.1007/s11664-011-1853-0
34. Simmons G, Wang H (1971) Single crystal elastic constants and calculated aggregate properties: a handbook, 2nd edn. The MIT Press, Cambridge
35. Schmidt RD, Case ED, Ni JE et al (2013) High-temperature elastic moduli of thermoelectric $SnTe_{1\pm x-y}SiC$ nanoparticulate composites. J Mater Sci 48:8244–8258. doi:10.1007/s10853-013-7637-6
36. Shin C-S, Gall D, Hellgren N et al (2003) Vacancy hardening in single-crystal TiN_x(001) layers. J Appl Phys 93:6025–6028. doi:10.1063/1.1568521
37. Portnoi KI, Mukaseev AA, Gribkov VN, Levinskii YV (1968) Modulus of normal elasticity of porosity-free titanium and zirconium nitrides. Sov Powder Metall Met Ceram 7:406–408. doi:10.1007/BF00774537
38. Jiang X, Wang M, Schmidt K et al (1991) Elastic constants and hardness of ion-beam-sputtered TiN_x films measured by Brillouin scattering and depth-sensing indentation. J Appl Phys 69:3053–3057. doi:10.1063/1.348963
39. Wang Y, Duncan K, Wachsman E, Ebrahimi F (2007) The effect of oxygen vacancy concentration on the elastic modulus of fluorite-structured oxides. Solid State Ion 178:53–58. doi:10.1016/j.ssi.2006.11.003
40. Bloem J, Kröger FA (1955) A relation between hardness and stoichiometry in lead sulphide single crystals. Nature 175:861. doi:10.1038/175861a0
41. Rice RW, Wu CC, Borchelt F (1994) Hardness-grain-size relations in ceramics. J Am Ceram Soc 77:2539–2553. doi:10.1111/j.1151-2916.1994.tb04641.x